Recalibrating Quantum Error- correcting Codes in the Presence of High-Weight Errors

November 2019

Abstract. Existing quantum computing devices cannot support fault-tolerant preparation of logical qubit state protected quantum error-correcting code. Therefore, it is difficult to accurately estimate the failure rate of encoded gates whose operand logical qubits are pre-loaded with large state-preparation noise. We articulate a scheme of decoupling transversal encoded gate errors from state-preparation noise and experimentally validate its use-case for IBMQ quantum processors. We find that in the absence of state preparation noise, the IBMQ processors significantly raise the likelihood of certain two-qubit errors in the operand(s) of [[7, 1, 3]] transversal gates. Yet, we show that encoding can still improve the gate fidelity provided that the gate operands are strategically decoded/corrected for the likely two-qubit errors in lieu of their less probably single-qubit counterparts. This trade-off enables quantum CSS code to principally correct longer strings of errors without increasing the codeword size and paves new avenues of achieving fault-tolerance in the era of noisy intermediate scale quantum computers.

1. Introduction

Accurate characterization of encoded gate noise in the logical qubit, realized on recently unveiled publicly accessible and other quantum processors, is a challenging yet promising avenue of research experiments [36, 43, 39, 24, 40, 31]. The challenge lies in distinguishing errors in the encoded gate, from those in the faulty state-preparation of its logical operands. Encoding physical qubits into high fidelity logical state remains at odds with hardware limitations including (i) limited number of ancillary qubits and (ii) sparse qubit-qubit connectivity [15, 33, 45]. These constraints enact unreliable non-local CNOT gates on the encoding qubits, leading to the preparation of noisy encoded state, particularly in case of universal quantum error-correcting code. Recently, a pioneering attempt [18] of preparing $[[5, 1, 3]]$ encoded basis state has reported state-preparation fidelity no higher than 0.57 on 5-qubits superconductor quantum processor. However, the principle robustness of encoded gate protected universal quantum error-correcting code, can still be demonstrated, provided that large state-preparation noise can be effectively discounted.

Conventional schemes of decoupling gate errors from state preparation noise, such as randomized benchmarking [16, 28, 13, 44] or their variant [10] for encoded gates, become ineffective once the fidelity-decay curve no longer depends on the length of randomized gate sequence and reduces to a function of state-preparation noise only [32].

Error probability distribution, estimated by these schemes, would likely conceal *intrinsic hardware errors* i.e. errors which cannot be ascribed to the non-fault-tolerant attributes of quantum circuit. Some common sources of intrinsic errors include qubits leakage, cross-talk, systematic under- or over-rotation, non-unitary and non-Markovian noise. At the same time, these challenges also open new window of opportunity—to rethink ways of uncovering intrinsic errors and calibrating existing fault-tolerance schemes in the light of more realistic noise models. Both aspects of the problem are crucial to advance state-of-art in the Noisy Intermediate Scale Quantum Computer [35] (NISQ) era.

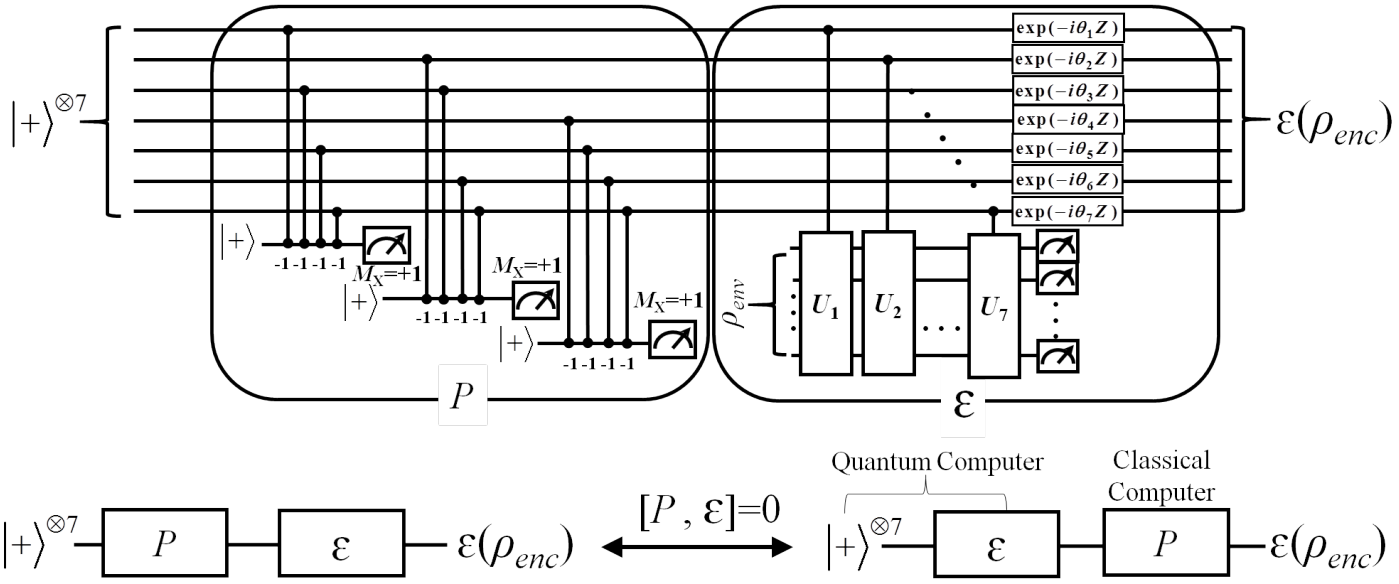

Figure 1. Commute-Back Noise Operator Propagation Method circumvents encoded state preparation for obtaining logical Identity gate error statistics. Noise corrupted $[[7, 1, 3]]$ encoded $|+\rangle$ state can be envisioned as an equal superposition state subject to non-unitary codespace P, followed by application of identity gate noise operator ε. If $[P, \varepsilon] = 0$ then noise operator ε commutes back to act on the superposition state. In case of dephasing channel, the controlled-U_i becomes controlled rotation about Z-axis. After obtaining ε induced probability distribution of phase-flip errors in superposition state from experimental statistics, the subsequent mapping of these errors onto encoded $|+\rangle$ state is offloaded to classical post-processing step which implements ideal projection P. The commutation relation $[P, \varepsilon] = 0$, provides reliable and efficient experimental means of indirectly computing phase-flip error probability distribution of the logical state. Please refer to Section-3 for more details

A two-fold contribution of this work is follows. First, it provides efficient experimental means of indirectly estimating probability distribution of errors (pde) of the transversal logical (encoded) operand of the logical gate. This pde can be further analyzed for likelihood of correctable and un-correctable errors which arise due the faulty logical gate. The scheme does not require encoded state preparation, instead, it suffices to transversally initialize the encoding qubits into equal superposition state.

Small error rates (of the order 10^{-3} or less) of the single qubit rotation gates enable reliable preparation of equal superposition state of multiple qubits on many quantum computing platform including IBMQ devices. By contrast, encoded state preparation, involving just as many encoding qubit, usually results in poor fidelity state due far more unreliable two-qubit gates (error rates of a CNOT gate easily exceeds 10^{-2} on IBMQ and other relevant platforms). Therefore, noisy logical gate ε is directly applied to the superposition state and pde is computed by transversally measuring encoding qubits in X-basis. This pde is obtained from experimental statistics and is transformed into the pde of noisy encoded operand by using codespace projector P. A remarkable feature of this method is that it offloads the most complicated part associated with logical state preparation—the projective transformations of superposition state and its pde—onto classical post- processing, leaving quantum device tasked with only transversal gates execution.

The validity of proposed scheme is conditioned upon $[P, \varepsilon] = 0$ whereby ε commutes back to act on the qubits equal superposition state. Fig-1 shows canonical form of ε thats fulfills the commutation relationship and models both unitary [20, 23] and non-unitary component noise operations in a real quantum hardware such as superconductors. It generalizes the unified noise model $\varepsilon(\rho) = e^{-i\theta Z}(p\rho + (1-p)Z\rho Z)e^{i\theta Z}$ given in Ref [30], to include component non-unitary noise operations other than dephasing, such as depolarizing noise channel. Indeed, for the case of dephasing channel, the general controlled-unitary gates $U_1, U_2, \ldots, U_7$ reduce to corresponding controlled rotation about Z-axis applied to the environment ρ_{env} in Fig-1. It is easy to see from the figure that when ε represents noisy logical identity gate, it commutes with projector P of Steane $[[7, 1, 3]]$ logical $|+\rangle$ state. The commutation becomes feasible by virtue of (i) valid back-propagation of ε operations ($e^{-i\theta Z}$ and controlled-unitary gates) through the control operands of CNOT gates in P. Remarkably, the commutation relationship can be shown for some non-trivial cases such as Steane CNOT gate with its operands initialized in standard logical basis states (e.g $|+\rangle$,$|-\rangle$) used in our experiment results. For Steane Identity and CNOT gate, the commutation assumption can be easily extended to include spatially and temporally correlated (e.g. non-Markovian) noise models realized in Ref [2]. Other correlated noise models are also admissible as long as $[P, \varepsilon] = 0$ is satisfied. That is when proposed method obtains reliable estimate of errors probability distribution.

Secondly, we analyze the error probability distribution and show that Steane [38] logical gate significantly elevates the likelihood of certain two-qubit errors in the operand. These are degenerate errors and can be easily corrected when converted into non-trivial (other than Identity) codespace Stabilizers. Appendix A provides proof-of-principle examples of distance-3 CSS codes [8] capable of correcting weight-2 bit-flips/phase-flips or both. All two-qubit errors in case of Steane code can be corrected, although, at the expense of their corresponding co-syndrome single-qubit counterparts transform into logical errors. We find that the gate can achieve higher fidelity by virtue of encoding if, instead of dogmatically decoding its operand for single-qubit errors—as

occurs in conventional fault-tolerant schemes—a given syndrome is decoded into more likely two-qubit errors instead of less probable single-qubit error. In comparison to the strict single-qubit decoding schemes, our proposed strategy achieves 2-3 fold reduction in the logical failure probability of the operand. It is the probability that decoding and correction of errors reveals the intended logical state in classical post-processing. Most importantly, this multi-fold reduction provides critical leverage to demonstrate that Steane code can practically improve the gate fidelity, although only modestly.

Organization of remaining discussion is follows: Section-2 situates this work within relevant prior studies on fault-tolerance and error-correction in real quantum computers. Section-3 delineates the framework of experimentally calculating pde in the encoded operands. The details of experiment setup are given in Section-4. Experimental results and their discussion constitute Section-5 while Section-6 concludes the manuscript with possible directions of the future work.

2. Motivation of this work

The theory of fault-tolerant quantum computation [27] allows quantum error correction to lower decoherence rate of the encoded qubit by preventing faulty gate operations to accumulate errors on the encoding qubits. Founded on the assumptions that qubit-environment interaction keeps decoherence rate per qubit below certain limit [1, 4] and confines errors to exponentially small subset of qubits, it has naturally steered conventional error-correction schemes towards correcting logical qubit for small number of encoding qubits in errors—the defining attribute of the local noise model [4, 41]. Unfortunately, real quantum hardware invalidate these assumptions by significantly raising decoherence levels among certain qubits and elevating joint probability of noisier qubits in error [43]. Such behavior is clearly visible in qubits error probability distribution shown in Fig-2. The distribution is obtained from the results of two flagship experimental circuit (one applies transversal CNOT gates and other applies sequence of Identity gates) on two different IBMQ devices (ibmq_16_melbourne and ibmqx4_tenerife). In comparison to that of several single qubit errors (e.g. qubit-8 in ibmq_16_melbourne and qubit-2 in ibmqx4_tenerife), the joint failure of noisier qubit pairs (1, 11) and (4, 5), occurs with significantly higher probability and may contradict local noise assumption.

For a distance $d = (2d_e - 1)$ code, an occurrence of errors on d_e or more codeword qubits likely belongs to a set of uncorrectable error events that result in the incorrect decoding of faulty qubits, followed by undetectable alteration of the logical qubit state during recovery phase. If a quantum hardware distributes decoherence rates unevenly among the encoding qubits, the likelihood of logical qubit failure is at least the joint probability of d_e noisiest qubits failing to escape uncorrectable errors. For example, if we assume that each qubits set in Fig-2, represents a logical qubit protected by three-qubit phase-flip code, the logical failure probability will be dictated by elevated likelihood of errors on frequently failing qubit pairs (1,11 in experiment (a)) and (4,5

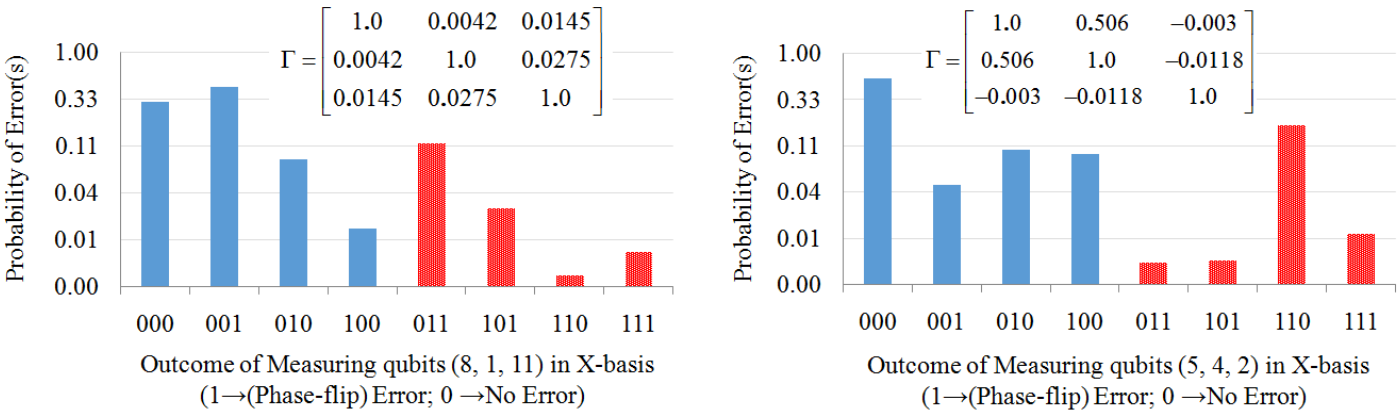

(a) Transversal CNOT gate in ibmq_16_melbourne

(b) Memory (Identity) gate in ibmqx4_tenerife

Figure 2. (Color online) The probability distribution (shown using logarithmic ordinates) over the phase-flipped qubits in an IBM Superconductor quantum computers. Both circuits prepared their qubits in equal superposition state and Measured these in X-basis after their respective gates. Two or more qubit errors are shown by red textured bars while fewer than two errors are represented by solid blue bars. In (a) ibmq_16_melbourne qubits 1,8 and 11 were control operand of three CNOT gates. Their corresponding target qubits were 0, 7 and 3, each prepared in equal superposition state. In (b) we applied a sequence of 24 Identity gates to each one of the qubits 2,4 and 5 on ibmqx4_tenerife device. Ideally, both circuits stabilize initial state (i.e. $|+\rangle$) of the qubits. However, the decoherence due to real noisy gates, was projected onto phase-flip errors when qubits were Measured in the X-basis. The qubit phase-flip error probabilities were obtained using 8192 x 3 = 24576 shots for each circuit. The Pearson correlation matrix Γ obtained from respective Measurement statistics, indicates spatial correlations among qubits errors

in experiment (b)). Whenever this joint failure probability exceeds un-encoded qubit error probability, the encoding can only increase decoherence rate of logical qubit. That is when error-correction becomes counterproductive by gathering errors faster than the rate of their correction. To date, practical quantum error-detection [11, 25, 36] and correction [12, 34, 22] have shown qualified success in counteracting noise patterns in real quantum computers.

Thus, it comes as no surprise that only a few studies have attempted to evaluate fault-tolerance on recently showcased quantum computing devices that can easily fit Gottesman's $[[4, 2, 2]]$ encoded qubit [19]. Among these studies, even fewer [42, 31, 21, 40] have managed to show that encoded qubits and gates exhibit higher fidelity. However, Gottesman's $[[4, 2, 2]]$ being an error-detecting code, finds limited applications in a more realistic scenario in which logical qubit can only be discarded upon final read-out instead of on each occasion when an error has been detected. For practical purposes, error-correction is expected to remain an indispensable tool of increasing the longevity of the logical qubit subject to real noisy environment, though its applicability and efficacy

largely remains an unexplored avenue of investigation. This paper shows that expected gains of quantum fault-tolerance can still be recovered in practical quantum computing device and the fidelity of logical qubit can be higher than that of un-encoded qubit, provided that one is not afraid of correcting d_e or more errors even with distance-d code.

The manuscript defines *high-weight errors* as at least $d_e = (\frac{d+1}{2})$ bit-flips/phase-flips/both bit-and-phase-flip occuring in the logical qubit (otherwise these are termed *low-weight errors*). In a logical qubit codeword, the high-weight errors can combinatorially outnumber all possible combinations of stabilizer measurements outcomes, each one maps to a set $\mathcal{S}$ of syndrome-indistinguishable high-weight errors. This, however, does not erect fundamental impediment to error-correction, as long as the $\mathcal{S}$ constitutes a set of degenerate errors i.e. they all convert logical codespace to the same coset and vice-versa. Hence, any displacement in logical qubit state due to an error in $\mathcal{S}$, can be offset by another error from the set, applied as recovery operation. Their joint action recovers the noiseless state of the logical in a way that is subtly different from conventional error correction protocol. While latter attempts to uniquely decode an error for its self-cancellation (Identity operation $\longrightarrow$ trivial Stabilizer), the high-weight error correction recovers the noiseless logical state by generally stitching together different strings of errors to construct an appropriate codespace stabilizer (non-trivial stabilizer/gauge operator).

A given syndrome can be decoded into either low-weight or high-weight errors for correction, although strictly low-weight (conventional) error-correction would eliminate the second choice. Suppose that Fig-2 error probabilities belonged to the encoding qubits (1,8,11) of three-qubit repetition phase-flip code, then likely noise behavior motivates us to decode certain syndromes into two-qubit errors. For example, correcting qubits-(1,11) versus correcting qubit-8 in Fig-2(a) and correcting qubits-(4,5) versus correcting qubit-2 in Fig-2(b), would lower the logical failure probability (=0.056) below the un-encoded qubit error probability (=0.156); the relevant calculations and comparison details can be found in Section-5. Therefore, by selectively decoding syndromes into likely set of high-weight errors in place of less probable low-weight counterpart, the principle advantage of quantum error-correction may be restored even if faultier codeword qubits frequently fail simultaneously regardless of their error correlations (compare Γ for the two cases in Fig-2). For logical gates protected by phase-flip repetition code/ Steane [38] ([[7, 1, 3]]) code, our experiments show that selective high weight error-correction can provide two- to three-fold reduction in logical failure probability in comparison to the case when only low-weight errors are corrected. We anticipate that presented strategy can help fault-tolerance regain its ground in the unfolding NISQ era which is expected to unleash frequently occurring many-qubits errors [37] in the quantum computers. Note that for the remainder of manuscript, the so called High-Weight EC is synonymous with selective high-weight error-correction as has been exemplified in the discussion so far.

3. Calculating Phase-Flip Error Distribution for the Steane Encoded State

The illustrate this method by using Steane ($[[7, 1, 3]]$) code. The Steane encoded $|+\rangle$ state contains equal superposition of all sixteen codewords of classical $[7, 4, 3]$ Hamming code $\mathbf{C}_1$. Its dual code $\mathbf{C}_2 = \mathbf{C}_1^{\perp} \subset \mathbf{C}_1$ is a classical $[7, 3]$ code (minimum code-distance $= 3$) whose codewords constitute the support of X- and Z-Stabilizers of the Steane code. It is a distance-3 code and was originally invented to correct arbitrary single-qubit errors. However, Appendix A shows that it is possible to correct arbitrary two-qubit errors by sacrificing corresponding single-qubit error-correction. The trade-off provides leeway to select dominant high-weight errors for correction for optimizing the fidelity of Steane encoded gates. Note that only phase-flip errors are taken into consideration in our experimental results and analysis, because of their decisive role in limiting the overall/average gate fidelity.

Fig-1 outlines Noise Operator Commute-Back method as experimental means of calculating probability distribution over errors in Steane logical gates by initializing its operand(s) in the equal superpositon state: $\rho_{sup} := \otimes_{i=1}^{7} |+\rangle\langle+|$ (where $|+\rangle := \frac{1}{\sqrt{2}}(|0\rangle + |1\rangle)$). The preparation of a operand logical states $\rho_{enc} := |\bar{+}\rangle\langle\bar{+}| = \frac{1}{16}\sum_{x,y\in\mathbf{C}_2^{\perp}} |x\rangle\langle y|$ proceeds by applying an ideal codespace projection P to ρ_{sup}, which converts it into the ρ_{enc}. (later, it will be shown how projection part can be simulated as classical post-processing step). Afterwards, as encoded state undergoes processing, the corresponding noisy logical gate operator ρ_{enc} may commute back to act on superposition state ρ_{sup} if $[P, \varepsilon] = 0$. This crucial commutation property lies at the heart of this work and on the fact that dephasing, being recognized as the most potent source of noise in transmon superconductor qubits [9, 29, 26], can be described as qubit-environment interaction shown in Fig-1 and Fig-4 for logical identity and CNOT gate respectively. Hence these logical gates can be directly applied to ρ_{sup} state and error statistics can be collected from the transversal Measurement of operand constituent physical qubits. These statistics are converted into error probability distribution of encoded operand state ρ_{enc} by simulating ideal code-space projection P applied to ρ_{sup} carrying phase-flip errors.

The equal superposition state requires only single qubit Hadamard gates which can be executed with very high fidelity—their failure probability is reported to be an order of magnitude smaller than that two-qubit gates and measurements in IBM calibration data. The execution time of single qubit-rotation gates (usually in ns) is negligibly small compared to decoherence time constant T2 (typically in tens of μs) which attributes lower decoherence noise to Hadamard gate. Therefore, small infidelity of superposition state can be safely ignored compared to those in case when qubits site idle for several no-ops(identity gates) or undergo CNOT gates. One caveat regarding phase-flip errors decoding is the readout noise which can significantly vary across IBMQ qubits—by nearly an order of a magnitude. This limits the choice of our operand qubits to those with acceptable readout failure probability. Alternatively, we either apply IBMQ readout noise compensation scheme or indirectly Measure qubit error by propagating these to qubits having lower readout noise. Corresponding experiment

setup and relevant constraints are elaborated in the next section. For now, we return to the development of analytical tool for computing probability distribution of phase-flip errors.

3.1. Noise Operator Commute-Back Method

Define vector $\mathbf{k} \in \mathbb{Z}_2^7$ that identifies phase-flip errors in $|\bar{+}\rangle$ state by setting corresponding indices of error- and error-free qubits to 1 and 0 respectively. The calculation of probability distribution over set $\mathbf{k}$ phase-flipped qubits in the noisy $|\bar{+}\rangle$, can be parsed into three-step procedure (1) preparation of an ideal encoded state $\rho_{enc} = |\bar{+}\rangle\langle\bar{+}|$ (2) Applying noise to ρ_{enc} and obtain noisy $\varepsilon(\rho_{enc})$ state (3) measuring the resulting noisy state for $\mathbf{k}$ errors. The $\rho_{enc} = \frac{1}{16}\sum_{x,y\in\mathbf{C}_2^\perp}|x\rangle\langle y|$ is prepared by projecting equal superposition state of seven qubit $\rho_{sup} = |+\rangle^{\otimes 7}$ onto $[[7,1,3]]$ codespace by using ideal projection P. We first write density matrix of ideal encoded state as

$$\rho_{enc} = 8P\rho_{sup}P^\dagger$$

Where pre-factor 8(=1/0.125) comes from the denominator in quantum Measurement expression that outputs ρ_{enc} with probability 0.125. Upon successful projection, the addition of noise converts the state into $\varepsilon(\rho_{enc})$. The probability $\Pr_{\mathbf{k}}$ that $\mathbf{k}$ qubits are phase-flipped in the noisy state is calculated by using quantum measurement expression:

$$\Pr_{\mathbf{k}} = \mathrm{tr}(M_{\mathbf{k}}M_{\mathbf{k}}^\dagger\varepsilon(\rho_{enc}))$$

where $M_{\mathbf{k}} = \frac{1}{16}\sum_{x,y\in\mathbf{C}_2^\perp}(-1)^{\mathbf{k}.(x\oplus y)}|x\rangle\langle y|$. Express ρ_{enc} in the form of ρ_{sup} to rewrite above expression as:

$$\Pr_{\mathbf{k}} = 8\mathrm{tr}(M_{\mathbf{k}}M_{\mathbf{k}}^\dagger\varepsilon(P\rho_{sup}P^\dagger)) \tag{1}$$

When noise operator ε commutes with P, it enables crucial reordering of operators in (1) so that experimentally infeasible preparation of ρ_{enc} state can be avoided. Then, reordering peddled by $[\varepsilon, P] = 0$, yields

$$\Pr_{\mathbf{k}} = 8\mathrm{tr}(M_{\mathbf{k}}M_{\mathbf{k}}^\dagger P\varepsilon(\rho_{sup})P^\dagger) \qquad \therefore [\varepsilon, P] = 0 \tag{2}$$

Being interested in phase-flipped errors only, we expand Kraus operator representation of $\varepsilon(\rho_{sup})$ such that each operator $Z_i = \sum_{x\in\mathbb{Z}_2^7}(-1)^{i.x}|x\rangle\langle x|$ flips qubits specified by the binary vector i, in the ρ_{sup} state with probability p_i i.e. $\varepsilon(\rho_{sup}) = \sum_{i\in\mathbb{Z}_2^7} p_i Z_i\rho_{sup}Z_i^\dagger$ where $\sum_{i\in\mathbb{Z}_2^7} Z_iZ_i^\dagger = I$. Substituting $\varepsilon(\rho_{sup})$ in (2) and bringing P, $P^\dagger$ inside the summation will give

$$\Pr_{\mathbf{k}} = 8\mathrm{tr}(M_{\mathbf{k}}M_{\mathbf{k}}^\dagger\sum_{i\in\mathbf{C}_2^\perp} p_i PZ_i\rho_{sup}Z_i^\dagger P^\dagger)$$

Note that p_i is an experimentally measurable quantity and our goal is write $\Pr_{\mathbf{k}}$ in terms of p_i. It is clear from Fig-1 that $\forall_i\ [P, Z_i] = 0$, since phase errors in ρ_{sup} commute with

the controlled-Z gates implementing P, and enter ρ_{enc} untransformed. Swap P with Z_i (thus also $P^\dagger$ with $Z_i^\dagger$), bring trace operator, $M_{\mathbf{k}}, M_{\mathbf{k}}^\dagger$ inside the summation and invoke permissible reordering of matrices insider trace operator to obtain:

$$\begin{aligned}\Pr_{\mathbf{k}} &= 8\sum_{i\in\mathbf{C}_2^\perp} p_i \mathrm{tr}(M_{\mathbf{k}} Z_i P \rho_{sup} P^\dagger Z_i^\dagger) \\ &= \sum_{i\in\mathbf{C}_2^\perp} p_i \mathrm{tr}(M_{\mathbf{k}} Z_i \rho_{enc} Z_i^\dagger)\end{aligned}$$

where we have used the fact that $M_{\mathbf{k}}$ is hermitian and $M_{\mathbf{k}}M_{\mathbf{k}}^\dagger = M_{\mathbf{k}}$. Write trace input as product of two summations i.e. $M_{\mathbf{k}} Z_i \rho_{enc} Z_i^\dagger = \frac{1}{256}\sum_{u\in\mathbf{C}_2^\perp}(-1)^{u.(i\oplus\mathbf{k})}\sum_{x,y\in C}(-1)^{\mathbf{k}.x\oplus i.y}|x\rangle\langle y|$. The first summation is non-zero only when $i\oplus\mathbf{k}\in\mathbf{C}_2$. This leads to $\sum_{u\in\mathbf{C}_2^\perp}(-1)^{u.(i\oplus\mathbf{k})} = |\mathrm{C}_2^\perp| = 16$ and $\sum_{x,y\in\mathbf{C}_2^\perp}(-1)^{\mathbf{k}.x\oplus i.y}|x\rangle\langle y| = Z_i\rho_{enc}Z_i^\dagger$ since $(-1)^{\mathbf{k}.x\oplus i.y} = (-1)^{\mathbf{k}.x\oplus\mathbf{k}.y}$. Hence

$$M_{\mathbf{k}} Z_i \rho_{enc} Z_i^\dagger = \begin{cases} Z_i\rho_{enc}Z_i^\dagger & i\oplus\mathbf{k}\in\mathrm{C}_2 \\ 0 & \text{otherwise}\end{cases}$$

Since $\mathrm{tr}(Z_i\rho_{enc}Z_i) = 1$, the final expression of $\Pr_{\mathbf{k}}$ simplifies to

$$\Pr_{\mathbf{k}} = \sum_{i|i\oplus k\in\mathbf{C}_2} p_i \tag{3}$$

Therefore, the probability distribution over $\mathbf{k}$ phase-flipped qubits in the $n-$qubits encoded state can be calculated from the probability distribution (p_i) of phase-flipped qubits in the $n-$qubits equal superposition sate which can be transversally prepared on the quantum processor hardware. Finally, it can be seen that same procedure applies to $|-\rangle$ logical state. In this case the encoding qubits are initialized in phase-flipped equal superposition $|-\rangle^{\otimes 7}$ state.

3.2. Comparison with Randomized Benchmarking Schemes

It might be worth comparing Noise Operator Commute-Back method with randomized benchmarking based schemes on the grounds of their common objective—the calculation of (encoded or un-encoded) gate failure probability. Large state-preparation noise [32] and un-modeled unitary (coherent) errors [30] leads to inaccurate estimate of gate error rates in randomized benchmarking. The Commute-Back Noise Operator method addresses these shortcomings by averting encoded state preparation and including both coherent and incoherent components of noise. However, unlike randomized benchmarking, its scope is limited by operators commutation constraint $[P,\varepsilon] = 0$. While randomized benchmarking is vulnerable to correlations among errors [6], our method is more general and admits spatial-temporal correlations in the noise model. An example noise operator of this type is illustrated in Ref [2]. Finally, the proposed method still needs to be iterated over all possible combinations of basis states–like quantum process tomography–for profiling an overall (or average) gate error rate. By contrast, randomized benchmarking can generate such profile more efficiently.

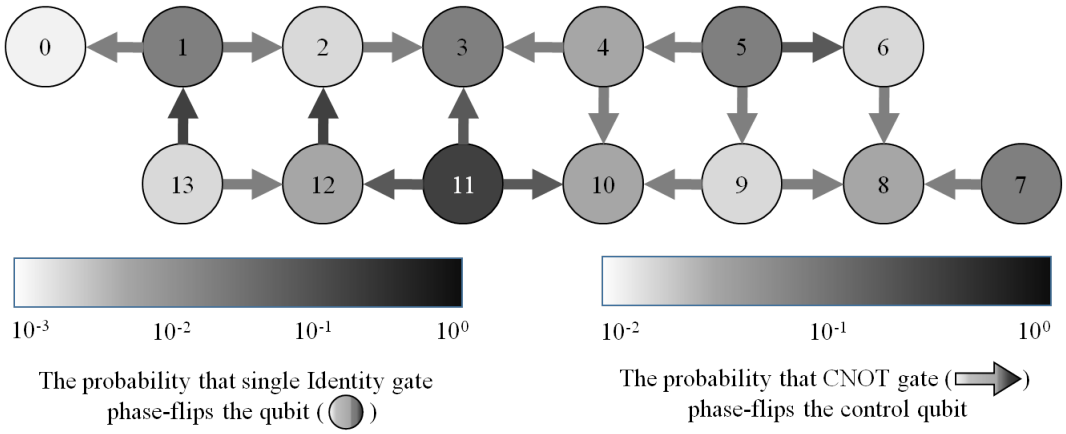

Figure 3. The error probability of ibmq_16_melbourne qubits (shaded circles) due to (a) Single Identity gate (b) CNOT gates (shaded arrows). These probabilities were obtained from Qiskit (https://qiskit.org) quantum state tomography routine. Although, these error-probabilities varied over time, this snapshot is most consistent with our experimental results and recent IBMQ calibration data. Note that the indicated error probabilities include respective qubit state-initialization and read-out errors

4. Experiment Setup

We designed our experiments for investigating errors in the $[[7, 1, 3]]$ encoded qubit subject to logical CNOT and Memory (Idle) gate. The nature of logical operations dictated the choice of quantum computing device–expected to be large enough to store at least two logical qubits and facilitated sufficiently large number of transversal physical CNOT gates. Another selection problem was the identification of operand physical qubits suitable for achieving considerably higher gate fidelity by High-Weight EC. We generated error profile of physical qubits and gates so that these could be discriminated on the basis of their respective noise levels. For quantitative comparison, we defined *fidelity gain* as the ratio of logical failure probability of Low-Weight EC to the logical failure probability of High-Weight EC. We noticed that fidelity gain was highlighted when logical operand contained noisier physical qubits in certain *optimal* proportions. Based on selective operand compositions, our experimental results showed that strict single-qubit error-correction frequently failed to reduce the logical failure probability of the encoded gate below the break-even point i.e. average failure probability of corresponding un-encoded gates (the discussion on computing this crucial parameter will appear shortly). By contrast, strategic correction of likely two-qubit errors achieved far more encouraging results by frequently lowering the logical failure probability below the break-even point.

4.1. Selecting the Quantum Computing Device

At the time of writing, the ibmq_16_melborune 14-qubits superconductor quantum computer was the largest IBMQ quantum computer in our access, that could store two $[[7, 1, 3]]$ logical qubits and execute its logical CNOT gate with a minor constraint to be discussed later. The device features ease of programming, accessibility, daily calibration, fast execution of quantum circuits and reproducibility of their results. Our six months long experimental study of this machine began soon after its introduction in Nov 2018. Nearly 500 experiments were spent in rigorously authenticating the substantial disparity in qubits decoherence levels. Although, bulk of our final results summarize findings from the most recent set of executions, large number of earlier experiments proved handful in systematically identifying an appropriate set of noisy qubits set (and CNOT gates) to constitute credible evidence of high-weight errors and the fidelity gain obtained by their correction.

4.2. Scheduling Experiments Around Device Calibration

The computer maintenance routine, in the form of periodic device calibration, significantly dictated the schedule our experiments. We note that the qubits error probability generally increased with the time elapsed since last calibration, mainly due to its increasing accumulated usage. Apparently, this two hours long process runs special quantum state and process tomographic routines to benchmark decoherence levels in the hardware and reboots the device after retuning and refreshing the qubits. During the calibration interval, the device does not perform user experiments, instead, these are stored as long queue of pending jobs. Once calibration is complete, the device forthwith resumes execution of pending user experiments, the first job in the queue is likely executed with highest quality qubits and gates. To minimize the time-dependent coherence loss effect, we attempted to carefully schedule our experiments in order to minimize their wait time in the queue. To further increase the validity of our results displayed in Section-5, each data point on the graph was collected from the median output of at least three different executions of the exact same logical gate circuit.

4.3. Generating Qubits Errors Profile

The IBMQ platform also updates device calibration data quantifying noise levels in the form of average-case error probability. Although, average-case data is a valuable indicator of an overall performance of circuit components (qubits and gates), we independently generated their error profile based on the specific needs of our experiment setup. The profile was generated by running quantum state tomography routine provided by the Qiskit (https://qiskit.org) platform. It computed the likely density matrix of the qubit prepared in equal superposition state subject to memory or CNOT gate, both would ideally leave its state unchanged. The Fig-3 uses gray-scale image to identify higher decoherence noise with dark shaded circles (qubits) and arrows (CNOT

gates). It shows that qubit-11 is the noisiest qubit followed by qubits 1, 3 and 7. The indicated error probabilities were statistically computed by counting the fraction of times a qubit prepared in the $|+\rangle$ state, collapsed to -1 eigenstate of X operator upon Measurement i.e. it acquired phase-flip error. On the other hand, the CNOT gate induced qubit error probability was calculated from the statistical likelihood of the control qubit flipping from $|+\rangle$ to $|-\rangle$ state when both its operand qubits were initialized in $|+\rangle$ states. It was also obtained by quantum state tomography of the control qubit as it undergoes following circuit: State initialization→ CNOT→Measurement. From the comparison given in the map, the CNOT gates specified by their (control, target) qubit pairs (13,1), (12, 2) (11,3), (11,10) and (11,12) are more likely to phase-flip their control operand than the rest. Note that the likelihood of faulty state initialization and Measurement is included in the qubit error-probabilities of shown in Fig-3. Nevertheless, the error probability profile generated by our statistics are in close agreement with those published on the IBMQ website.

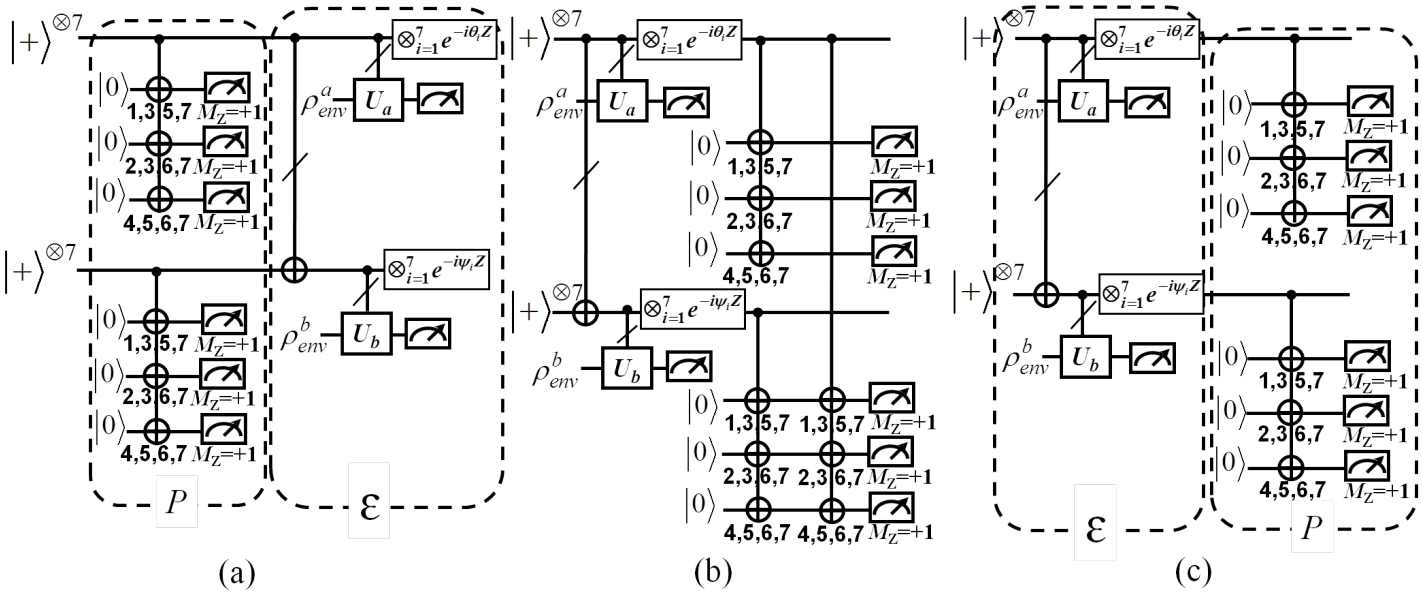

Figure 4. Noise operator commute-back procedure for estimating error probability distribution in the noisy Steane CNOT gate. In (a) the noisy CNOT ε is applied to the encoded state $|+\rangle$ obtained by projecting superpositon state onto codespace by the projector P. This is equivalent to first applying ε to the superposition state, followed by its projection (by applying P) onto the code-space. We ascribe this reordering is to an important property of CNOT gates: CNOT(op_1, op_2) CNOT(op_2, op_3) = CNOT(op_1, op_3) CNOT(op_2, op_3) CNOT (op_1, op_2) shown in (b). Afterwards (b) reduces to (c) since P remains unchanged by the superfluous joint projection of both operands onto the codespace. Note that P is considered ideal projection and it is simulated in the classical post-processing, whereas, ε is enacted in quantum hardware

4.4. Calculating Failure Probabilities

The error-correction logical failure probability of the Steane code utilizes expression given in (3). Define $\Pr^{(0)} := \Pr_{\mathbf{k}=0}$ and $\Pr^{(\mathbf{L})} := \sum_{\mathbf{k}:\mathbf{H}_2^{\perp}\mathbf{k}=0,|\mathbf{k}|=3} \Pr_{\mathbf{k}}$ as probabilities of no error and *all* undetectable logical errors, respectively. Similarly, define $\Pr_{\mathbf{k}}^{|\mathbf{k}|=1} := \Pr_{\mathbf{k}:|\mathbf{k}|=1}$ and $\Pr_{\mathbf{k}}^{|\mathbf{k}|=2} := \Pr_{\mathbf{k}:|\mathbf{k}|=2}$ as probabilities of single-qubit and two-qubit errors respectively; the binary vector $\mathbf{k}$ locates error qubits in the codeword by 1 at the corresponding indices. These probabilities can be easily derived from (3). Then, by definition, the logical failure probability of Low-Weight EC (P_{lw}) becomes:

$$P_{lw} = \sum_{\mathbf{k}} \Pr_{\mathbf{k}}^{|\mathbf{k}|=2} + \Pr^{(\mathbf{L})} \tag{4}$$

Likewise, the logical failure probability of High-Weight EC (P_{hw}) will become:

$$P_{hw} = \sum_{c\in\mathbf{Z}_2^3} \min_{\mathbf{k}:\mathrm{H}\mathbf{k}=c} (\Pr_{\mathbf{k}}^{|\mathbf{k}|=1}, \sum_{\mathbf{m}:\mathbf{H}(\mathbf{m}+\mathbf{k})=0} \Pr_{\mathbf{m}}^{|\mathbf{m}|=2}) + \min(\Pr^{(0)}, \Pr^{(\mathbf{L})}) \tag{5}$$

The expression (5) represents convex optimization problem with simple solution. It says that one should prefer to correct two-qubit errors whenever their cumulative probability exceeds that of their low-weight counterparts. Next, in order to quantify the improvement (or degradation) in the fidelity of encoded gate when protected by error-correction, we compare the logical failure probability with un-encoded qubit error probability. However, the substantial disparity in physical error rates, complicates the selection of an appropriate statistical metric that faithfully mirrors the fidelity of physical gate which is un-encoded by definition. For comparison, we want a single figure of merit p_e to (i) reflect overall (in)fidelity of multi-qubit encoded state (ii) distributes overall infidelity *identically* among individual qubits on the basis of per-qubit error probability [2]. For transversal Steane gate, we mathematically define p_e as solution to following set of non-linear equations:

$$(1-p_e)^7 = \Pr^{(0)} \tag{6}$$

$$7p_e(1-p_e)^6 = \sum_{\mathrm{k}} \Pr_{\mathrm{k}}^{|\mathrm{k}|=1} \tag{7}$$

$$21p_e^2(1-p_e)^5 = \sum_{\mathrm{k}} \Pr_{\mathrm{k}}^{|\mathrm{k}|=2} \tag{8}$$

$$7p_e^3(1-p_e)^4 = \Pr^{(\mathrm{L})} \tag{9}$$

It is evident that p_e not only encapsulates error probability distribution of multi-qubit state and but also inherits a sense of per-qubit error probability. In practice, the four equality constraints from equations (6)—(9) generally lead to an approximate solution—one that minimizes the cumulative mean-square difference. The best p_e was computed by solving above set of equations as an instance of non-convex optimization, and provides

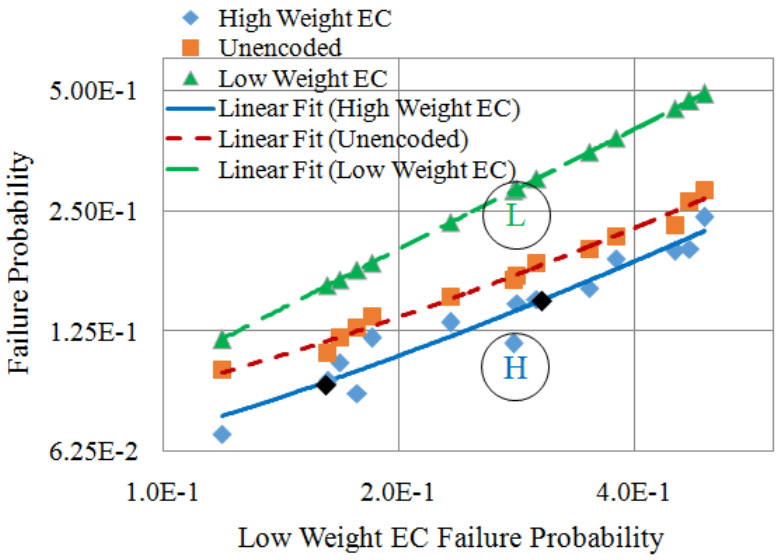

Low Weight Errors		High Weight Errors	
Error Qubit	Prob.	Error Qubits Pairs	Net Prob.
2	0.0097	(13,12), (5,6), (4,0)	0.146
4	0.022	(13, 5), (12,6), (2,0)	0.0355
12	0.23	(13, 2), (5,0), (4,6)	0.009
5	0.03	(13, 4), (2,6), (12,0)	0.015
0	0.0135	(13,6), (2,4), (12,5)	0.032
6	0.33	(13, 0), (12,4), (2,5)	0.015
13	0.137	(12,2), (4,5), (6,0)	0.021
None	0.238	Undetectable Logical Z Errors	0.009

Low Weight EC Failure Prob. at L is 0.283
High Weight EC Failure Prob. at H is 0.116

Figure 5. (Color online) Steane High-Weight EC lowers the failure probability of the CNOT gate for logical $|+\rangle$ state operands. Only control operand is referenced for comparison of failure probabilities. The graph plots triple (P_{hw}, p_e, P_{lw}) against P_{lw}. The triple plotted on the graph is the median of three triples, each obtained from encoded CNOT gate experiment results. Each experiment computed its triple from the statistics collected from 8192 executions(shots) of the same logical gate. The logical failure probabilities were computed from these statistics by using expression given in (4) and (5). For the encircled data points, the syndrome-wise comparison between single-qubit error and their corresponding two-qubit errors, is listed in the table (all errors in each row yield same syndrome value). The shaded rectangles present components of failure probability of High-Weight EC while those inside large thick outlined rectangle, represents components of Low-Weight EC failure probability

reference error-probability of un-encoded qubit, for comparison with P_{lw} and P_{hw} in Fig-5,6 and 7.

5. Experimental Results

The main objective of our experiments is the statistical calculation of logical failure probabilities for evaluating proposed error-correction scheme. Again, it is reminded that an error-correction procedure simply applies correction to the classical bit-string obtained from transversal Measurement of seven qubits initialized in the equal superposition state and processed by $[[7, 1, 3]]$ logical gates. We consider gate execution to be successful if its operand(s) corrected readout yields a codeword in C_2, otherwise, it is counted towards logical failure. By statistically calculating the fraction of instances resulting in logical failures, we obtain P_{lw} and P_{hw} as described in the previous section.

For the sake of completeness, we shall also include experiments in which operands encoded state preparation is not skipped. A CNOT gate protected by three-qubit

redundancy phase-flip code will be applied to the formally encoded operands. After the gate execution, the control operand undergoes complete decoding and allows its subsequent transversal Measurement to reveal errors therein. The readout result passes through error-correction and subsequently correlated with the correct outcome for calculating logical failure probability.

5.1. Logical CNOT

The first set of experiments is designed to calculate the probability distribution of the control operand of the Steane logical CNOT with both operands in the $|\bar{+}\rangle$ state. Based on the Section-3 analysis, actual preparation of logical state is not required, instead, gate can be directly applied to operand qubits initialized in equal superposition state as shown in Fig-4. The gate is mapped to the subset of seven (out of eighteen) device-level CNOT gates indicated by edges in Fig–3. The qubit-qubit connectivity constraints can be understood by visualizing the device as a directed graph mapping qubits and CNOT gates to its vertices and edges, respectively. The vertex(qubit) at the arrow head is the recommended target operand of the corresponding edge (CNOT gate). IBMQ platform invites users to achieve high fidelity gate execution by mapping operand qubits in recommended control-target order specified by edge direction. The accuracy of the gate may be slightly lower if it is executed while its operands are mapped opposite to the edge direction (arrow pointing towards control qubit). We relax the operand order constraint at the expense of incurring some nominal gate infidelity. Then, the edge direction becomes unimportant and directed graph turns into fully connected (undirected) graph allowing any pair non-adjacent qubits to undergo CNOT gate by means of successive swap gates. Although, this flexibility expands numerous permutations of encoding physical qubits placement, these can be shortlisted by the constraints of our experiment setup for logical CNOT gate, which require:

(i) Each constituent physical CNOT gate has unique control-target qubit pair.

(ii) None of the gates acts on non-adjacent qubit pair. Otherwise, arbitrating (non fault-tolerant) swap gate can convert single qubit error into multi-qubit errors.

The first requirement is relatively straightforward; it arises from the innate transversality of Steane CNOT gate, and can be readily fulfilled. However, the second condition cannot be entirely met due to the structure of device connectivity graph. Essentially, it requires that matching number (size of maximum independent edge set) of the graph is at least seven. However, it is easy to show that Fig-3 graph has matching number = 6. This means we can only execute six physical CNOT gates transversally satisfying both conditions. Our analysis shows that the missing gate barely alters our results and conclusions whenever its error probability is set to the average error-probability of other six gates. We validate this conclusion in the execution results to be described shortly. Before proceeding, we list typical gate operands in the form of (control, target) encoding qubit pairs, in the decreasing order of their contribution to the results:

- $\{(13,1),(12,2),(10,11),(4,3),(5,9),(6,8),(0,7)\}$
- $\{(13,1),(12,11),(2,3),(4,10),(5,9),(6,8),(0,7)\}$
- $\{(13,1),(12,11),(2,3),(4,5),(8,7),(9,10),(6,0)\}$
- $\{(1,2),(13,12),(11,3),(4,5),(6,8),(9,10),(0,7)\}$

The list shows that our preferred compositions of logical control operands, contains qubits bearing lower state initialization failure probability, for example: 0,2,4,6,9 and 13). It is because error statistics obtained from logical CNOT experiments ($|+\rangle^{\otimes 7}$ state-initialization $\rightarrow$ CNOT $\rightarrow$ Measurement) always contain some inseparable component of unwanted state initialization and Measurement errors. Selection of mentioned qubits ensures that the contribution of undesired error probability remains reasonably smaller—about an order of magnitude lower in comparison to that of the respective CNOT gates. All compositions allowed six transversal gates on adjacent qubits. How to deal with the gate on the non-adjacent qubit-pair? will be answered next.

The non-local CNOT is converted into classically-controlled NOT gate after commuting it with the subsequent operand X-basis Measurement. It flips the control qubit Meaurement result when target qubit is readout in $|1\rangle$ state. This additional transformation is also carried out off-line and precedes error-correction applied to the readout result in software post-processing. While this transformation adequately captures error propagation feature of the gate, it may fall short of capturing (phase) errors introduced by the gate itself. Fortunately, it is possible to compensate for the CNOT gate noise by pulling qubits having higher readout noise into the control operand of CNOT gate. In Fig-3 a large fraction of nosier qubits (dark shaded circles) also accrue large readout noise; their Measurement and CNOT error rates have comparable probabilities ranging: $2.5 \times 10^{-2} - 5 \times 10^{-2}$. Higher readout noise in the control qubit of the missing non-local CNOT gate, adequately compensates for the noise that would have been accumulated had the missing gate had been executed without relocating its operand qubits. Our experimental results show that the missing CNOT gate noise compensation does not substantially impact general trends of comparison between Low-Weight EC and High-Weight EC failure probabilities, (shown in Fig-5), to be described shortly. Therefore, although, majority of our data points are based on uncompensated CNOT configurations, a few compensated data points, both plotted and un-plotted, will be analyzed for their alignment with the general trend.

Fig-5 plots data triples (P_{hw}, p_e, P_{lw}) against P_{lw}. Each triple corresponds to median statistics of three logical CNOT experiments with same qubits composition of its operands. The three tuples (one from each CNOT experiment) were sorted by P_{hw} value and only median tuple was plotted on the graph. The comparison of logical failure probabilities evince fidelity gain of 2x–3x providing enough reduction to lower in P_{hw} just below p_e—the break-even point. Thus Steane code has improved the reliability of CNOT gate whose both operands are initialized in $|+\rangle$ state. Detailed insights can be obtained by comparing the logical failure

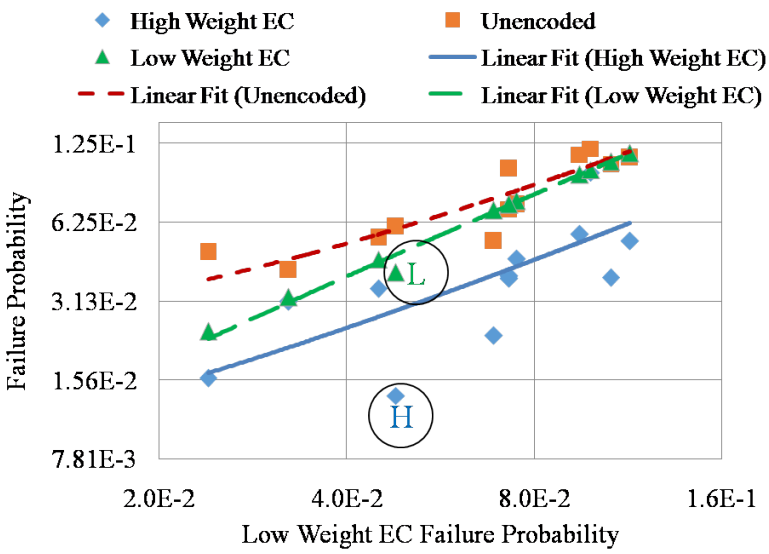

Low Weight Errors		High Weight Errors	
Error Qubit	Prob.	Error Qubits Pairs	Net Prob.
12	0.072	(13,10), (6,9), (5,0)	0.012
5	0.020	(13, 6), (10,9), (12,0)	0.002
10	0.238	(13, 12), (6,0), (5,9)	0.00036
6	0.007	(13, 5), (12,9), (10,0)	0.0022
0	0.0046	(13,9), (12,5), (10,6)	0.0035
9	0.0023	(13, 0), (10,5), (12,6)	0.0067
13	0.0019	(10,12), (5,6), (9, 0)	0.032
None	0.604	Undetectable Logical Z-Errors	0.0002

Low Weight EC Failure Prob. at L is 0.0482
High Weight EC Failure Prob. at H is 0.0136

Figure 6. (Color online) Extrapolation of Fig-5 in low-noise (Low-Weight EC failure prob. < 0.1) regime, was achieved by skipping some (but not all) CNOT gates. The missing gates were simulated as ideal CNOT gates (in classical post-processing) and corresponding both compensated and uncompensated triples points are included in the graph. Logistics of plotting the graph and calculations of probabilities remain the same as those described in Fig-5. The table shows breakdown of failure probabilities of encircled data points

probabilities of the triple ($P_{hw} = 0.116, p_e = 0.161, P_{lw} = 0.283$) for the gate operands composition:$\{(13,1),(12,11),(2,3),(4,10),(5,9),(6,8),(0,7)\}$. The table in Fig-5 elaborates breakdown of logical failure probabilities shown as encircled H and L data points for High- and low-Weight EC respectively.

The syndrome-wise comparison between single- and two-qubits error probabilities shows that qubits 13, 12 and 6 are distinctly noisier in the control operand; their two-qubit errors combinations e.g. (13,12),(13,6) and (12,6), are more probable then their corresponding single-qubit counterparts (qubits 2,4 and 0). By prioritizing the correction of faultier pair of qubits, significant reduction in P_{hw} becomes possible. Therefore, by virtue of High-Weight EC, control operand fails less frequently for encoded CNOT gates for all the triples. Furthermore, it should be noted that encircled data point does not aberrantly deviate from trend-line for compensated CNOT configuration. For example, when the operands qubits are swapped on the last pair and qubit-7 becomes control qubit (and 0 becomes target), then the high readout noise on qubit-7 adequately fills the shoes of missing CNOT gate. The corresponding triple simply drifts along the trend-line and is re-situated within close vicinity of existing triples. On one instance, the compensated version relocates it to ($P_{hw} = 0.092$, $p_e = 0.11$, $P_{lw} = 0.162$), on other, it maps it to ($P_{hw} = 0.16$, $p_e = 0.2$, $P_{lw} = 0.35$). Shown as black diamonds on the

Fig-5, both triples reinforce the existing trend-line. Thus, the figure accurately reflects the fidelity gain of High-Weight EC for the complete logical CNOT gate.

The missing CNOT problem actually proves to be a valuable tool of extrapolating Fig-5 curves for comparison in the low noise regime where $P_{lw} < 0.1$. When multiple physical CNOTs are replaced with ideal gates in post-processing, their corresponding control qubits gather lesser noise and lower P_{lw}. The corresponding p_e and P_{hw} values are shown in the Fig-6 for uncompensated version of logical CNOT. It shows that P_{hw} remains consistently lower than p_e and so do the smaller P_{hw} values. However, as their respective trend-lines approach 0.1, P_{lw} converges to p_e, while P_{hw} remains notably smaller as shown by the gap between corresponding trend lines at the end ($P_{lw} = 0.12$). Upon extrapolation in high-noise regime (higher P_{lw} values), these data triples and trend lines faithfully transform into those in Fig-5 (where $P_{lw} > 0.11$). The encircled data point presents an example in which two CNOT gates (12,2) and (11,10) were physically executed, whereas, the remaining five gates (13,1), (5,4), (6,8), (9,3), (0,7) were classically executed. The table shows that elimination of the two-qubit errors (12,5) and (10,12) at the expense of uncorrected co-syndrome single-qubit errors on qubits 9 and 13, provides nearly three-fold reduction on logical failure probability.

5.1.1. Suppression of Readout Noise Above results describe the performance of logical gate without taking target operand into consideration. However, since several qubits, with high readout noise, enter the target operand, it is important to correct the operand error probabilities for large readout noise. Fortunately, this can be efficiently accomplished by invoking Qiskit readout noise filtration routines. We apply these routines in a way that qubits readout noise was directly profiled by executing prescribed test circuits on the device hardware. For each set of seven physical qubits comprising the

Table 1. High-Weight error-corrected $[[7, 1, 3]]$ CNOT gate fails less often than physical CNOT gate. Both control and target operands are considered for comparison. The table lists readout-noise compensated probabilities, for selected control, target operands configurations used in Fig-5. Only one physical CNOT gate—on the non-adjacent qubits—was skipped from hardware execution in the first five table entries. The last logical CNOT, marked by *, executed all seven constituent gates

Composition of operands	Failure Probability					
	Control		Target		Overall	
Control , Target	Physical	Logical	Physical	Logical	Physical	Logical
$\{13, 12, 10, 5, 4, 9, 0\}, \{1, 2, 11, 6, 3, 8, 7\}$	0.251	0.152	0.066	0.043	0.3	0.188
$\{8, 5, 9, 4, 12, 13, 2\}, \{7, 6, 10, 3, 11, 1, 0\}$	0.116	0.076	0.05	0.027	0.161	0.101
$\{8, 9, 12, 13, 2, 4, 6\}, \{7, 10, 11, 1, 3, 5, 0\}$	0.115	0.06	0.047	0.002	0.156	0.061
$\{13, 12, 10, 4, 5, 6, 0\}, \{1, 2, 11, 3, 9, 8, 7\}$	0.144	0.009	0.139	0.063	0.262	0.071
$\{0, 2, 13, 10, 5, 6, 9\}, \{1, 3, 12, 11, 4, 8, 7\}$	0.1	0.046	0.121	0.026	0.208	0.071
$*\{7, 9, 12, 2, 4, 5, 13\}, \{8, 10, 11, 1, 3, 6, 0\}$	0.139	0.095	0.070	0.020	0.199	0.113

target operand, a total of 128 test circuits are executed. Apparently, each test initializes the qubits in one of 128 possible classical states (0000000...1111111) and Measure these in Z-basis to compute corresponding readout error-probability distribution. After computing a set of 128 distributions, one routine seems to register complete readout noise profile in the form of 128 x 128 conditional error probabilities. Another routine then uses this profile to correct the results of separately executed user-defined circuit to yield new statistics compensated for readout noise. The p_e and P_{hw} of the target operands of selected Fig-5 logical CNOT gates, are obtained from the readout noise compensated error probability distribution and listed in Table-1.

To show that high-weight error-correction improves the reliability of quantum gate, the overall P_{hw} of encoded CNOT gate must be less than the p_e value (average failure probability of un-encoded CNOTs). To this end, we also recompute control operand readout-noise compensated P_{hw} for the selected set of logical CNOT gates. The new P_{hw} of both logical operands and their corresponding p_e are also juxtaposed in Table-1. The comparison reveals that overall failure probabilities are smaller in case of encoded gates. The last entry of the table contains failure probabilities for the complete Steane CNOT gate executing all seven constituent physical gates. The seventh gate is a non-local gate containing non-adjacent operand qubits: 13 and 0. It was realized by applying local CNOT(13,1) after swapping qubits 1 and 0. The lower failure probability of complete Steane CNOT gate further reinforces the efficacy of High-Weight EC. Finally, we would like to point out that for logical $|-\rangle$ state operand(s), the elimination of high-weight errors features meaningful reduction in failure probability when $P_{hw} \geq 0.2$. Addressing this shortcoming paves an interesting avenue of further investigating proposed error-correction scheme.

5.2. Logical Memory

The memory errors arise due to the decoherence in logical operand as it undergoes sequence of identity (no-operation) gates. The complete experiment executes: State initialization $\rightarrow$ Identity gate sequence $\rightarrow$ Measurement. Before proceeding, we consider it important to point out a noteworthy behavioral variation observed in ibmq_16_melbourne qubits. In early days, the error-probabilities of device qubit, increased with the length of identity gates sequence. However, since May 4, 2019, this trend has been gradually fading—perhaps due to the systematic improvement in in qubits coherence time—and has now become somewhat difficult to reproduce. Yet, occasional device overuse still results in accelerated decoherence of more vulnerable qubits. Fig-7 shows data triples for various idle time intervals (ranging from single to 250 identity gates). Approximately half of all data triples predate May-4 and remain more or less trend-wise indistinguishable from those of later experiments. Several different subsets of seven qubits participated in the comparison, some of which are listed in the decreasing order of their contribution in the plots:

- $\{0, 7, 2, 11, 12, 8, 4\}$

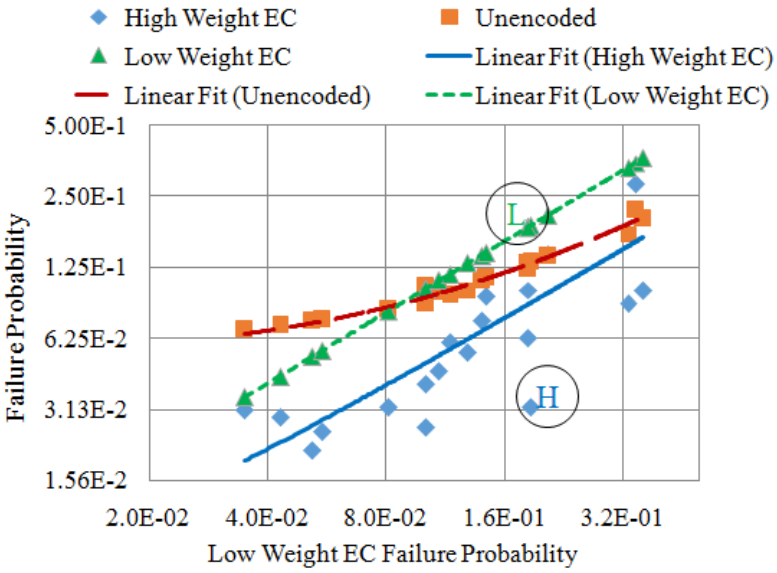

Low Weight Errors		High Weight Errors	
Error Qubit	Prob.	Error Qubits Pairs	Net Prob.
13	0.0083	(12,5), (11,3), (6,8)	0.0584
6	0.0034	(12,11), (5,3), (13,8)	0.048
5	0.1247	(12, 13), (11,8), (6,3)	0.0029
11	0.1635	(12, 6), (13,3), (5,8)	0.0034
8	0.0046	(12, 3), (13,6), (5,11)	0.0638
3	0.1069	(12, 8), (5,6), (13,11)	0.0035
12	0.0545	(13,5), (6,11), (3, 8)	0.0037
None	0.3479	Undetectable Logical Z -Errors	0.0019

Low Weight EC Failure Prob. at L is 0.186
High Weight EC Failure Prob. at H is 0.032

Figure 7. (Color online) High-Weight error-correction lowers the failure probability of $[[7,1,3]]$ encoded qubit in logical $|+\rangle$ state as it undergoes sequence of Identity gates (consisting of 1—250 gates). While Low-Weight EC becomes counterproductive ($P_{lw} > p_e$) after the cross-over point (intersection between p_e and P_{lw} trend-lines), High-Weight EC continues to keep P_{hw} lower than p_e before eventually converging to p_e at the end. Logistics of plotting the graph and calculations of probabilities remain the same as those described in Fig-5. The table shows breakdown of failure probabilities of encircled data points

- $\{1, 3, 7, 13, 11, 6, 5\}$
- $\{13, 12, 11, 3, 7, 6, 5\}$
- $\{13, 12, 11, 3, 8, 6, 5\}$

The figure shows that High-Weight EC provides significant fidelity gain for several values of P_{lw}. More crucially, it keeps logical failure probability below p_e even when $P_{lw} \geq p_e$. In this region, an encircled data point has been selected for deeper insight into the fidelity gain, while its comparison breakdown is shown in the table. The data point is an output of experiment (dated July 6) applying five identity gates to the qubits set $\{13, 12, 11, 3, 8, 6, 5\}$. In this case, the elevated likelihood of High-Weight errors can be ascribed to the joint failure of qubits selected from the subset $\{11, 5, 3\}$ containing three noisier qubits. The table shows that correcting logical operand for errors on qubit pairs (11,5),(11,3) and (3,5), in place of those on qubits 8, 13 and 6 delivers nearly six fold reduction in logical failure probability.

A crucial constraint in the logical memory experiment setup was the mitigation of readout noise due to the inclusion of several high state initialization and Measurement error encoding qubits (for example qubits: 1,3,7 and 11). If these qubits had been

directly (destructively) Measured, the likely read-out inaccuracy would have artificially raised the joint failure probability of two (or more) qubits. We solved this problem by deploying unused qubits for indirectly (non-destructively) Measuring dark shaded qubits (Fig-3) with higher accuracy. Fortunately, these auxiliary qubits (e.g. 0,2,8 and 10) contain lower state initialization/Measurement noise and can reliably replicate phase-error from memory (identity) gate qubits through the CNOT gate (whose control operand is the auxiliary qubit initialized in the $|+\rangle$ state, the memory qubit acts as target operand). A good indicator of reduction in readout noise is the decrease in P_{lw} since inflated high-weight error probability is discounted. Therefore, non-destructive Measurements were applied whenever reduction in P_{lw} was possible. It lowers the failure probabilities in several triples including $(P_{hw} = 0.0625, p_e = 0.125, P_{lw} = 0.18)$ for the experiment containing memory qubits set $\{1, 12, 11, 3, 7, 6, 5\}$. In this case, auxiliary qubits: 0, 13, 10, 2 and 8 destructively Measure memory qubits: 1,12,11,3 and 7 respectively, reducing triple to $(P_{hw} = 0.045, p_e = 0.098, P_{lw} = 0.109)$. Yet, High-Weight EC continues to lower the decoherence rate of logical memory.

Finally, it should be noted that Qiskit readout noise compensation routines can be used to further suppress the readout noise. Preliminary comparative analysis reveals that enhanced noise reduction lowers all the curves in Fig-7 by approximately the same factor and does not introduce meaningful change in their overall trends. Since the principle advantage of High-Weight EC remains intact, therefore, these plots become somewhat superfluous and have been excluded from the manuscript.

5.3. Logical CNOT gate on Formally Encoded Qubits Protected by Three-qubit Phase-flip Code

The last set of experiments is relevant to the Gottesman's criterion of validating fault-tolerance in encoded quantum circuit with error-correction embedded in decoding and classical post processing. The comparison takes into account all the operational noise components that can arise in an encoded circuit, for example, state-preparation, logical gate, state decoding and readout errors. The criterion says that encoding is useful only if logical circuit raises the overall probability of obtaining correct output, higher than that of un-encoded circuit. If the correct output of the circuit is known apriori, then by comparing the ideal and actual outputs, the accumulated errors may be indirectly interpreted and corrected while decoding (and Measuring) the output logical qubits. The general sequence of Gottesman's validation scheme becomes: Encoded State preparation $\rightarrow$ Encoded quantum gates $\rightarrow$ State Decoding and Read-out. For example, if we design a test circuit which prepares encoded qubit ($|0\rangle \rightarrow |+++\rangle$) state to become an operand of logical identity gate, errors can be decoded from the parity calculations : X_1X_2 and X_2X_3 from the X-basis transversal Measurements of encoding qubits: X_1, X_2 and X_3. It is important to note that, contrary to the constraints of our experiment setup, the Gottesman sequence admits non-fault tolerant encoded state-preparation.

We demonstrate the effectiveness of High-Weight EC in protecting control operand

of CNOT gate using three-qubit phase-flip code. It encodes $|0\rangle_L \rightarrow |++\rangle$ and $|1\rangle_L \rightarrow |--\rangle$, where $|-\rangle := \frac{1}{\sqrt{2}}(|0\rangle - |1\rangle)$. Let $|x\rangle := \alpha_1|0\rangle_L + \beta_1|1\rangle_L$ and $|y\rangle := \alpha_2|0\rangle_L + \beta_2|1\rangle_L$ denote states of two encoded qubits, where $|\alpha_1|^2 + |\beta_1|^2 = 1$ and $|\alpha_2|^2 + |\beta_2|^2 = 1$. Then logical CNOT with control operand $|x\rangle$ and target operand $|y\rangle$, becomes transversal CNOT gate with opposite operands roles: qubits containing $|y\rangle$ control their corresponding targets in $|x\rangle$. Our experiment prepared both operands $|x\rangle$ and $|y\rangle$ in $|+\rangle_L = \frac{1}{\sqrt{2}}(|0\rangle_L + |1\rangle_L)$ and dispatched these to the encoded CNOT gate for processing. After the execution, the state of control operand (i.e. $|x\rangle$) decoded by applying encoding circuit in reverse. Afterwards, the disentangled physical qubits were transversally Measured in X-basis in order to obtain probability distribution over phase-flip errors and hence the likelihood of control operand logical failure. However, the Measurement results are corrected for errors before calculating the logical failure probabilities. In case of High-Weigth EC, the output is strategically corrected for frequently arising two-qubit errors and the overall logical failure probability is calculated accordingly. The qubit sets $\{4, 5, 6\}$ and $\{10, 9, 8\}$ held states $|x\rangle$ and $|y\rangle$ respectively. This allocation ensured that initialization and Measurement noise in qubits remained significantly lower than that in the CNOTs gates. The errors probability distribution was derived from the transversal Measurement of $\{4, 5, 6\}$ in X-basis after decoding. The detailed comparison among candidate error-correction scheme is shown in Fig-8. It is clear that High-Weight EC lowers the logical failure probability by trading less likely error on qubit-6 with more probable joint errors on 4 and 5. The table shows the breakdown of 1.6x fidelity gain for the encircled data point.

The plot also contains three horizontal lines acting as yardsticks of the fidelity gain (or loss) achieved from error-correction schemes. These lines represent average failure probability of un-encoded control operand of the physical CNOT gate, in descending order, such that qubit-5 is most noisy and qubit-6 is least noisy on average. These average probabilities were obtained from the statistics of separate set of experiments which replaced all encoded operations with un-encoded operations. More specifically, we calculated the likelihood of the failure of control qubits 4,5 and 6, from the execution of their CNOT gates targeting qubits 10, 9 and 8 respectively. The un-encoded operands of physical CNOT gate were initialized in the equal superposition state and transversally Measured in X-basis after the application of gate. The comparison between data points and horizontal lines shows that High-Weight EC successfully reduces logical failure probability below the average error-probability of the least noisy qubit (i.e. qubit 6) in 70% of our experiments. On contrary, the failure probability of Low-Weight EC exceeds qubit-6 error probability threshold in more than 90% of experiments. This presents strong experimental evidence that High-Weight EC can be used to improve the robustness against noise, as required by the Gottesman fault-tolerance criterion.

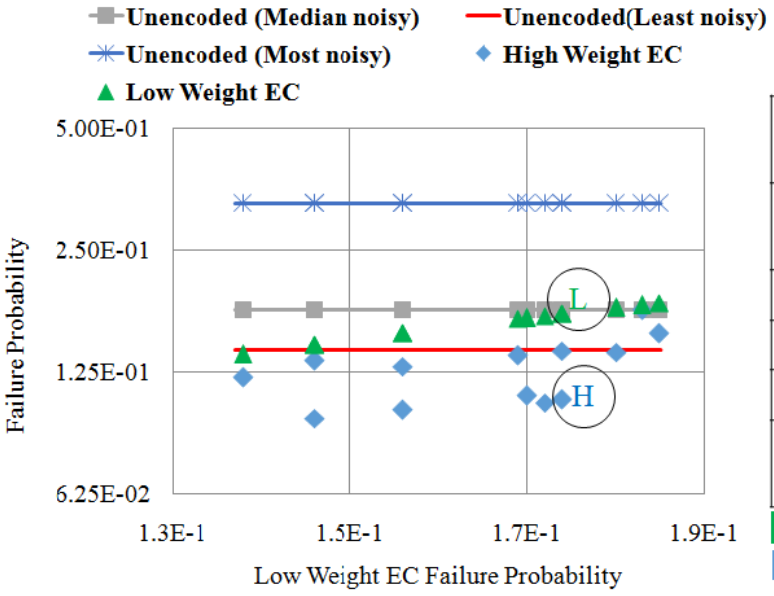

Low Weight Errors		High Weight Errors	
Error Qubit	Prob.	Error Qubits Pairs	Net Prob.
5	0.304	(4, 6)	0.021
4	0.101	(5, 6)	0.029
6	0.024	(4, 5)	0.091
None	0.4	Logical Z-Errors	0.032

Low Weight EC Failure Prob. at L is 0.174

High Weight EC Failure Prob. at H is 0.106

Figure 8. (Color online) High-Weight EC lowers CNOT gate failure probability, protected by the three-qubits repetition phase-flip code. Both operands were initialized in the logical $|+\rangle$ state, however, after the application of logical gate, only control operand was decoded and subsequently Measured for comparison of failure probabilities. Horizontal lines correspond to the un-encoded CNOT control operand average error probability and define thresholds for comparison with the encoded version. When protected by High-Weight EC, encoded operand qubit fails less frequently compared to the least noisy (lowest line) un-encoded operand qubit. Each plotted data point represents the median failure probability of three experimental results. Each result consisted of Measurement statistics collected from 8192 executions(shots) of the same logical CNOT circuit. For the encircled data points, the syndrome-wise comparison between single-qubit error and their corresponding two-qubit errors, is listed in the table (all errors in each row yield same syndrome value). The shaded rectangles present components of failure probability of High-Weight EC while those inside thick outline rectangle, represent components of Low-Weight EC failure probability

6. Conclusion

Error correction is an indispensable tool of protecting quantum information from noise. In this paper we presented a novel approach of error-correction, that convert errors into non-trivial code space Stabilizers. It allows quantum error-correcting codes to correct longer strings of errors contrary to what has been previously envisioned. The efficacy of proposed approach was validated by experiments on IBMQ quantum processor executing [[7, 1, 3]] noisy logical gates. These experiments were designed to indirectly infer probability distribution of errors in the logical gate operand, from the Measurement of encoding qubits after the application of gate. Remarkably, these qubits were not required

to encode experimentally infeasible [[7, 1, 3]] logical state, instead, their initialization in an equal superposition state sufficed. In this sense, the logical state-preparation errors were discounted from distribution; however, errors in qubits initialization logical and Measurements were duly taken into consideration.

In this setting, our experimental results showed that the new approach led encoded circuit to output intended state with higher probability in comparison with that of corresponding un-encoded circuit. For completeness, we included an experiment with full encoded state preparation—a logical CNOT applied to fully encoded three-qubit repetition phase-flip code. We found that the scheme performed equally well, adequately fulfilling fault-tolerance criterion for the encoded control operand. Although this work delineates novel approach of countering noise patterns expected in NISQ era devices, we believe that it merits further investigations on device technologies other than superconductors. In particular, what type of device-specific environments raise high-weight noise floor to justify application of proposed scheme? Apparently, if decoherence rates shrink in future, multi-qubit errors are unlikely to sustain large enough value, unless qubits and gates correlate their errors or establish their interdependencies in some unforeseeable mechanism. Moreover, the fault-tolerant preparation of a logical state, protected by full error-correcting code, has remained a daunting task to date. These and other relevant challenges indeed deserve more insights and tools to achieve fault-tolerance in real quantum processor.

Acknowledgments

Authors thank Arthur Robert Calderbank for sharing his feedback on the manuscript. The research was funded by Higher Education Commission Pakistan, under Startup Research Grant Program (SRGP) No.21-1843.

References

[1] Dorit Aharonov and Michael Ben-Or. Fault-tolerant quantum computation with constant error. In *Proceedings of the twenty-ninth annual ACM symposium on Theory of computing*, pages 176–188. ACM, 1997.

[2] Muhammad Ahsan and Syed Abbas Zilqurnain Naqvi. Performance of topological quantum error correction in the presence of correlated noise. *Quantum Information & Computation*, 18(9&10):743–778, 2018.

[3] Panos Aliferis and Andrew W. Cross. Subsystem fault tolerance with the bacon-shor code. *Phys. Rev. Lett.*, 98:220502, May 2007.

[4] Panos Aliferis, Daniel Gottesman, and John Preskill. Quantum accuracy threshold for concatenated distance-3 codes. *arXiv preprint quant-ph/0504218*, 2005.

[5] Dave Bacon. Operator quantum error-correcting subsystems for self-correcting quantum memories. *Physical Review A*, 73(1):012340, 2006.

[6] Harrison Ball, Thomas M Stace, Steven T Flammia, and Michael J Biercuk. Effect of noise correlations on randomized benchmarking. *Physical Review A*, 93(2):022303, 2016.

[7] Sergey B Bravyi and A Yu Kitaev. Quantum codes on a lattice with boundary. *arXiv preprint quant-ph/9811052*, 1998.

[8] A Robert Calderbank and Peter W Shor. Good quantum error-correcting codes exist. *Physical Review A*, 54(2):1098, 1996.

[9] Zijun Chen. *Metrology of quantum control and measurement in superconducting qubits*. PhD thesis, UC Santa Barbara, 2018.

[10] Joshua Combes, Christopher Granade, Christopher Ferrie, and Steven T Flammia. Logical randomized benchmarking. *arXiv preprint arXiv:1702.03688*, 2017.

[11] Antonio D Córcoles, Easwar Magesan, Srikanth J Srinivasan, Andrew W Cross, Matthias Steffen, Jay M Gambetta, and Jerry M Chow. Demonstration of a quantum error detection code using a square lattice of four superconducting qubits. *Nature communications*, 6:6979, 2015.

[12] Julia Cramer, Norbert Kalb, M Adriaan Rol, Bas Hensen, Machiel S Blok, Matthew Markham, Daniel J Twitchen, Ronald Hanson, and Tim H Taminiau. Repeated quantum error correction on a continuously encoded qubit by real-time feedback. *Nature communications*, 7:11526, 2016.

[13] Andrew W Cross, Easwar Magesan, Lev S Bishop, John A Smolin, and Jay M Gambetta. Scalable randomised benchmarking of non-clifford gates. *npj Quantum Information*, 2:16012, 2016.

[14] Eric Dennis, Alexei Kitaev, Andrew Landahl, and John Preskill. Topological quantum memory. *Journal of Mathematical Physics*, 43(9):4452–4505, 2002.

[15] Gerhard W Dueck, Anirban Pathak, Md Mazder Rahman, Abhishek Shukla, and Anindita Banerjee. Optimization of circuits for ibm's five-qubit quantum computers. In *2018 21st Euromicro Conference on Digital System Design (DSD)*, pages 680–684. IEEE, 2018.

[16] Joseph Emerson, Robert Alicki, and Karol Życzkowski. Scalable noise estimation with random unitary operators. *Journal of Optics B: Quantum and Semiclassical Optics*, 7(10):S347, 2005.

[17] Austin G Fowler. Analytic asymptotic performance of topological codes. *Physical Review A*, 87(4):040301, 2013.

[18] Ming Gong, Xiao Yuan, Shiyu Wang, Yulin Wu, Youwei Zhao, Chen Zha, Shaowei Li, Zhen Zhang, Qi Zhao, Yunchao Liu, et al. Experimental verification of five-qubit quantum error correction with superconducting qubits. *arXiv preprint arXiv:1907.04507*, 2019.

[19] Daniel Gottesman. Quantum fault tolerance in small experiments. *arXiv preprint arXiv:1610.03507*, 2016.

[20] Daniel Greenbaum and Zachary Dutton. Modeling coherent errors in quantum error correction. *Quantum Science and Technology*, 3(1):015007, 2017.

[21] Robin Harper and Steven T Flammia. Fault-tolerant logical gates in the ibm quantum experience. *Physical review letters*, 122(8):080504, 2019.

[22] L Hu, Y Ma, W Cai, X Mu, Y Xu, W Wang, Y Wu, H Wang, YP Song, C-L Zou, et al. Quantum error correction and universal gate set operation on a binomial bosonic logical qubit. *Nature Physics*, 15(5):503, 2019.

[23] Eric Huang, Andrew C Doherty, and Steven Flammia. Performance of quantum error correction with coherent errors. *Physical Review A*, 99(2):022313, 2019.

[24] Julian Kelly, R Barends, AG Fowler, A Megrant, E Jeffrey, TC White, D Sank, JY Mutus, B Campbell, Yu Chen, et al. State preservation by repetitive error detection in a superconducting quantum circuit. *Nature*, 519(7541):66, 2015.

[25] Julian Kelly, Rami Barends, Austin G Fowler, Anthony Megrant, Evan Jeffrey, Theodore C White, Daniel Sank, Josh Y Mutus, Brooks Campbell, Yu Chen, et al. State preservation by repetitive error detection in a superconducting quantum circuit. *Nature*, 519(7541):66, 2015.

[26] Morten Kjaergaard, Mollie E Schwartz, Jochen Braumüller, Philip Krantz, Joel I-Jan Wang, Simon Gustavsson, and William D Oliver. Superconducting qubits: Current state of play. *arXiv preprint arXiv:1905.13641*, 2019.

[27] Emanuel Knill and Raymond Laflamme. Theory of quantum error-correcting codes. *Physical Review A*, 55(2):900, 1997.

[28] Emanuel Knill, Dietrich Leibfried, Rolf Reichle, Joe Britton, R Brad Blakestad, John D Jost, Chris Langer, Roee Ozeri, Signe Seidelin, and David J Wineland. Randomized benchmarking of quantum gates. *Physical Review A*, 77(1):012307, 2008.

[29] Philip Krantz, Morten Kjaergaard, Fei Yan, Terry P Orlando, Simon Gustavsson, and William D Oliver. A quantum engineer's guide to superconducting qubits. *Applied Physics Reviews*, 6(2):021318, 2019.

[30] Richard Kueng, David M Long, Andrew C Doherty, and Steven T Flammia. Comparing experiments to the fault-tolerance threshold. *Physical review letters*, 117(17):170502, 2016.

[31] Norbert M Linke, Mauricio Gutierrez, Kevin A Landsman, Caroline Figgatt, Shantanu Debnath, Kenneth R Brown, and Christopher Monroe. Fault-tolerant quantum error detection. *Science advances*, 3(10):e1701074, 2017.

[32] Easwar Magesan, Jay M Gambetta, and Joseph Emerson. Characterizing quantum gates via randomized benchmarking. *Physical Review A*, 85(4):042311, 2012.

[33] Atsushi Matsuo, Wakakii Hattori, and Shigeru Yamashita. Reducing the overhead of mapping quantum circuits to ibm q system. In *2019 IEEE International Symposium on Circuits and Systems (ISCAS)*, pages 1–5. IEEE, 2019.

[34] Nissim Ofek, Andrei Petrenko, Reinier Heeres, Philip Reinhold, Zaki Leghtas, Brian Vlastakis, Yehan Liu, Luigi Frunzio, SM Girvin, L Jiang, et al. Extending the lifetime of a quantum bit with error correction in superconducting circuits. *Nature*, 536(7617):441, 2016.

[35] John Preskill. Quantum computing in the nisq era and beyond. *arXiv preprint arXiv:1801.00862*, 2018.

[36] Joschka Roffe, David Headley, Nicholas Chancellor, Dominic Horsman, and Viv Kendon. Protecting quantum memories using coherent parity check codes. *Quantum Science and Technology*, 3(3):035010, 2018.

[37] Daan Staudt. The role of correlated noise in quantum computing. *arXiv preprint arXiv:1111.1417*, 2011.

[38] Andrew Steane. Multiple-particle interference and quantum error correction. In *Proceedings of the Royal Society of London A: Mathematical, Physical and Engineering Sciences*, volume 452, pages 2551–2577. The Royal Society, 1996.

[39] Maika Takita, Andrew W Cross, AD Córcoles, Jerry M Chow, and Jay M Gambetta. Experimental demonstration of fault-tolerant state preparation with superconducting qubits. *Physical review letters*, 119(18):180501, 2017.

[40] Maika Takita, Andrew W Cross, AD Córcoles, Jerry M Chow, and Jay M Gambetta. Experimental demonstration of fault-tolerant state preparation with superconducting qubits. *Physical review letters*, 119(18):180501, 2017.

[41] Barbara M Terhal and Guido Burkard. Fault-tolerant quantum computation for local non-markovian noise. *Physical Review A*, 71(1):012336, 2005.

[42] Christophe Vuillot. Error detection is already helpful on the ibm 5q chip. *arXiv preprint arXiv:1705.08957*, 2017.

[43] Christophe Vuillot. Is error detection helpful on IBM 5q chips? *Quantum Information & Computation*, 18(11&12):949–964, 2018.

[44] Joel J Wallman, Marie Barnhill, and Joseph Emerson. Robust characterization of leakage errors. *New Journal of Physics*, 18(4):043021, 2016.

[45] Alwin Zulehner, Alexandru Paler, and Robert Wille. An efficient methodology for mapping quantum circuits to the ibm qx architectures. *IEEE Transactions on Computer-Aided Design of Integrated Circuits and Systems*, 2018.

Appendix A. Proof-of-Concept High-Weight Error Correction using Distance-3 CSS Codes

A distance-3 CSS code can decode single syndrome into multiple two-qubit errors. These can be corrected by mutually augmenting a pair of these errors to enact Stabilizer on the encoded state. This section exemplifies High-Weight error correction using Steane

Table A1. Correcting two-qubit phase-flip errors in $[[7,1,3]]$ code

Two phase-flips errors	Syndrome			Product of the pairs of phase-flips errors
	S_1^X	S_2^X	S_3^X	
(Z_1Z_2),(Z_5Z_6),(Z_4Z_7)	-1	-1	$+1$	$S_1^Z S_2^Z$, S_3^Z, $S_1^Z S_2^Z S_3^Z$
(Z_1Z_5),(Z_2Z_6),(Z_3Z_7)	$+1$	$+1$	-1	$S_1^Z S_2^Z$, S_1^Z, S_2^Z
(Z_1Z_3),(Z_5Z_7),(Z_4Z_6)	$+1$	-1	$+1$	S_1^Z, $S_1^Z S_3^Z$, S_3^Z
(Z_1Z_4),(Z_3Z_6),(Z_2Z_7)	-1	$+1$	-1	$S_1^Z S_3^Z$, S_2^Z, S_1^Z, S_2^Z
(Z_1Z_6),(Z_3Z_4),(Z_2Z_5)	-1	-1	-1	$S_1^Z S_3^Z$, $S_2^Z S_3^Z$, $S_1^Z S_2^Z$
(Z_1Z_7),(Z_2Z_4),(Z_3Z_5)	$+1$	-1	-1	$S_1^Z S_2^Z S_3^Z$, S_1^Z, $S_2^Z S_3^Z$
(Z_2Z_3),(Z_4Z_5),(Z_6Z_7)	-1	$+1$	$+1$	$S_2^Z S_3^Z$, S_2^Z, S_3^Z

$[[7,1,3]]$, Bacon-Shor $[[9,1,3]]$ and Kitaev $[[13,1,3]]$ surface code.

Appendix A.1. Steane $[[7,1,3]]$ *code*

The Steane code [8, 38], non-degenrate by design, can correct for arbitrary two-qubit errors. It confines logical qubit within the Stabilizer space spanned by six Stabilizers: $S_1^X : X_1X_3X_5X_7$; $S_2^X : X_2X_3X_6X_7$; $S_3^X : X_4X_5X_6X_7$; $S_1^Z : Z_1Z_3Z_5Z_7$; $S_2^Z : Z_2Z_3Z_6Z_7$; $S_3^Z : Z_4Z_5Z_6Z_7$. While correcting weight-2 errors, it becomes a degenerate code; the product of any two co-syndrome errors constitutes the Stabilizer operation on the code space. Table-A1 enumerate all possible weight-2 phase-flip errors. Each row lists degenerate errors along with their combinations leading to the non-trivial Stabilizers (trivial Stabilizers are omitted). Since all two-qubits bit- and phase-flip errors are shown to be corrected, therefore, Steane $[[7,1,3]]$ code corrects arbitrary two-qubit phase-flip errors. Likewise, it can be easily shown that it also corrects arbitrary two-qubit bit-flip errors.

Table A2. Gauge operators of $[[9,1,3]]$ Bacon-Shor code

X-Gauge operators		Z-gauge operators	
$G_{1,4}^X = X_1X_4$	$G_{2,5}^X = X_2X_5$	$G_{1,2}^Z = Z_1Z_2$	$G_{4,5}^Z = Z_4Z_5$
$G_{4,7}^X = X_4X_7$	$G_{5,8}^X = X_5X_8$	$G_{2,3}^Z = Z_2Z_3$	$G_{5,6}^Z = Z_5Z_6$

Appendix A.2. Bacon-Shor $[[9,1,3]]$ *code*

The nine-qubits Bacon-Shor code is a sub-system code [5] containing four stabilizers: $S_1^X : X_1X_2X_3X_4X_5X_6$, $S_2^X : X_4X_5X_6X_7X_8X_9$, $S_1^Z : Z_1Z_2Z_4Z_5Z_7Z_8$, $S_2^Z : Z_2Z_3Z_5Z_6Z_8Z_9$. It encodes five logical qubits; one belongs to the *system*, used for

storage and computation, while the rest comprise sub-system [3]. The state of system qubit remains unaffected by the applying logical X and Z gates to sub-system qubits. The Measurement of these logical operators, provides redundant means of syndrome extraction that gauges system for the presence of likely errors. The sub-system qubits are gauge qubits and their corresponding logical Pauli operations are gauge operators [3], listed in Table-A2. These can be leveraged to simplify the error correction procedure, might it be Low-Weight or High-Weight by nature. In latter case, these gauge operators compensate for the weight deficit when a pair of two-qubits errors to completes weight-6 Stabilizers. For Bacon-Shor code, the task of completing the code space stabilizer becomes a task of completing the its Stabilizer(s) modulo gauge operators.

A small subset of correctable two-qubits phase-errors are listed in Table-A4. It shows both the Stabilizers and concomitant gauge operators which become prominent when the pair of errors only enacts trivial Stabilizers on the code space (e.g. when $S_1^X = +1$ and $S_2^X = -1$). In general, these pairs comprise non-trivial Stabilizer upto appropriately chosen gauge operators. Finally, note that the table contains only handful of errors to exemplify proof-of-concept generalized error correction. However, like Steane code, it can be shown that one can correct arbitrary two-qubit errors in the Bacon-Shor code as well.

Appendix A.3. Kitaev $[[13, 1, 3]]$ *Surface code*

The surface codes [7], known for very high accuracy threshold [17, 14, 17], can efficiently decode errors on the codewords qubits, mapped to a two-dimensional grid, using nearest-

Table A3. Correcting two-qubit phase-flip errors in $[[13, 1, 3]]$ code

Two phase-flips errors	Syndrome						Product of the pairs of two phase-flips errors
	S_x^1	S_x^2	S_x^3	S_x^4	S_x^5	S_x^6	
(Z_4Z_6), (Z_7Z_9)	+1	-1	+1	-1	+1	+1	S_Z^3
(Z_4Z_9), (Z_6Z_7)	-1	-1	+1	-1	-1	+1	S_Z^3
(Z_4Z_9), (Z_6Z_9)	-1	+1	+1	+1	-1	+1	S_Z^3
(Z_5Z_7), (Z_8X_{10})	+1	+1	-1	+1	-1	+1	S_Z^4
(Z_5Z_{10}), (Z_7X_8)	+1	-1	-1	+1	-1	-1	S_Z^4
(Z_5Z_8), (Z_7Z_{10})	+1	-1	+1	+1	+1	-1	S_Z^4
(Z_9Z_{11}), $(Z_{10}Z_{13})$	+1	+1	+1	+1	-1	+1	$S_Z^5S_Z^6$
(Z_9X_{10}), $(X_{11}X_{13})$	+1	+1	+1	-1	+1	-1	$S_Z^5S_Z^6$
(Z_9Z_{13}), $(Z_{10}Z_{11})$	+1	+1	+1	-1	-1	-1	$S_Z^5S_Z^6$
(Z_1Z_3), (Z_4Z_5)	-1	+1	-1	+1	+1	+1	$S_Z^1S_Z^2$
(Z_1X_4), (Z_3Z_5)	+1	-1	+1	+1	+1	+1	$S_Z^1S_Z^2$
(Z_1Z_5), (Z_3Z_4)	-1	-1	-1	+1	+1	+1	$S_Z^1S_Z^2$

Table A4. Correcting two-qubit phase-flip errors in $[[9, 1, 3]]$ Bacon-Shor code

Syndrome	Two phase-flips errors	Stabilizers	Gauge Operators
$S_1^X = +1, S_2^X = -1$	(Z_1Z_4), (Z_2Z_5)	I	$G^Z_{1,2}, G^Z_{4,5}$
	(Z_2Z_5), (Z_3Z_6)	I	$G^Z_{2,3}, G^Z_{5,6}$
	(Z_1Z_5), (Z_3Z_6)	I	$G^Z_{1,2}G^Z_{2,3}G^Z_{5,6}$
$S_1^X = -1, S_2^X = +1$	(Z_5Z_8), (Z_4Z_7)	S^Z_1	$G^Z_{1,2}$
	(Z_5Z_8), (Z_6Z_9)	S^Z_2	$G^Z_{2,3}$
	(Z_4Z_9), (Z_6Z_7)	$S^Z_1S^Z_2$	$G^Z_{1,2}G^Z_{2,3}$
$S_1^X = -1, S_2^X = -1$	(Z_1Z_7), (Z_2Z_8)	S^Z_1	$G^Z_{4,5}$
	(Z_2Z_8), (Z_3Z_9)	S^Z_2	$G^Z_{5,6}$
	(Z_1Z_9), (Z_3Z_7)	$S^Z_1S^Z_2$	$G^Z_{4,5}G^Z_{5,6}$

neighbor parity check operations. The resulting local Stabilizer Measurements can not only correct less than d_e weight errors, but can also decode high-weight errors on the qubits located sufficiently far apart. In case of High-Weight error-correction, this spatial non-locality conditions resurfaces with far greater importance with crucial implications. On one hand, the local Stabilizer Measurement stipulates that the degenerate errors are located in vicinity to yield the same syndrome. On the other hand, these local errors can string a chain of faults realizing unwanted logical operation on the code space. Thus, while Table-A3 enumerates several correctable two-qubit phase-flip errors which can mutually constitute a Stabilizer operation, Fig-A1 depicts a situation in which a pair of these errors enacts logical-Z operation on the encoded qubit. This counter example shows that surface code [[13, 1, 3]] can only correct a subset of two-qubit errors.

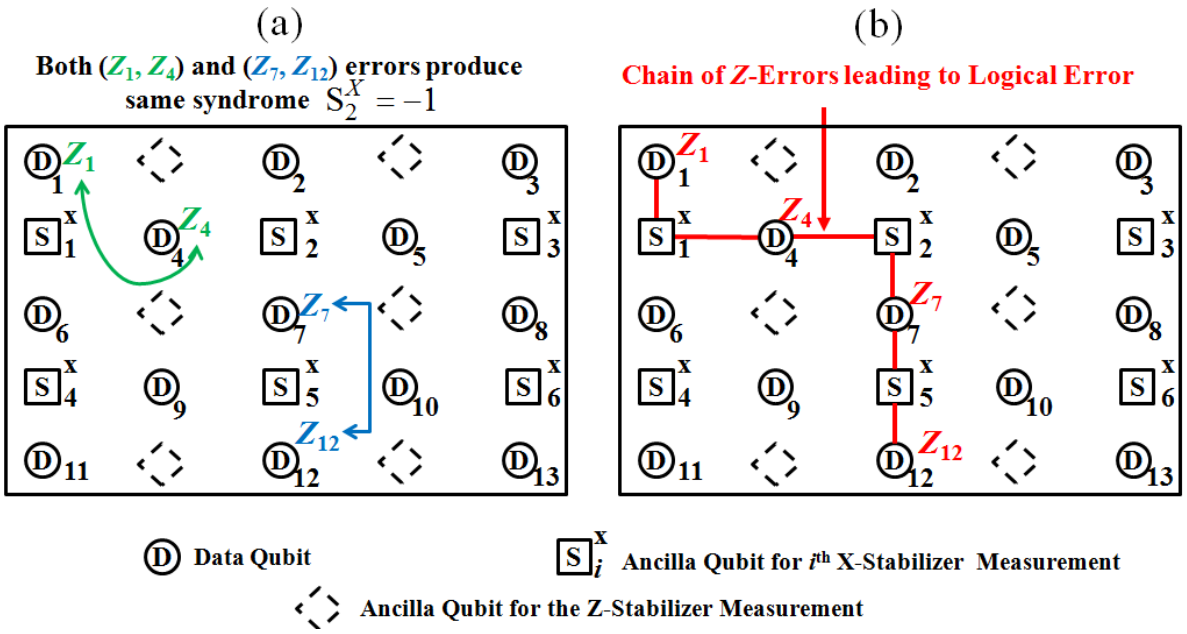

Figure A1. (Color online) A pair of co-syndrome two-qubit errors doesnot constitute Stabilizer operation. Instead, it afflicts logical Z-operation on the codespace. The counterexample example shows that surface code doesnot correct *arbitrary* two-qubit errors